frontiers | Frontiers in Marine Science

TYPE Original Research
PUBLISHED 06 August 2024
DOI 10.3389/fmars.2024.1444618

OPEN ACCESS

EDITED BY
Santhiyagu Prakash,
Tamil Nadu Fisheries University, India

REVIEWED BY
Ramasamy Ramasubburayan,
Saveetha University, India
Thirumurugan Durairaj,
SRM Institute of Science and Technology, India

*CORRESPONDENCE
Mostafa R. Abukhadra
Abukhadra89@Science.bsu.edu.eg
Stefano Bellucci
bellucci@lnf.infn.it

RECEIVED 06 June 2024
ACCEPTED 19 July 2024
PUBLISHED 06 August 2024

CITATION
Diab AS, Elsayed KNM, El-Sherbeeny AM, Al Zoubi W, Bellucci S and Abukhadra MR (2024) Synthesis and characterization of *Turbinaria ornata* mediated Zn/ZnO green nanoparticles as potential antioxidant and anti-diabetic agent of enhanced activity. *Front. Mar. Sci.* 11:1444618. doi: 10.3389/fmars.2024.1444618

Synthesis and characterization of *Turbinaria ornata* mediated Zn/ZnO green nanoparticles as potential antioxidant and anti-diabetic agent of enhanced activity

Amira S. Diab[1], Khaled N. M. Elsayed[2], Ahmed M. El-Sherbeeny[3], Wail Al Zoubi[4], Stefano Bellucci[5]* and Mostafa R. Abukhadra[1,6]*

[1]Materials Technologies and their Applications Lab, Geology Department, Faculty of Science, Beni-Suef University, Beni suef, Egypt, [2]Botany and Microbiology Department, Faculty of Science, Beni-Suef University, Beni suef, Egypt, [3]Industrial Engineering Department, College of Engineering, King Saud University, Riyadh, Saudi Arabia, [4]Materials Electrochemistry Laboratory, School of Materials Science and Engineering, Yeungnam University, Gyeongsan, Republic of Korea, [5]Istituto Nazionale di Fisica Nucleare (INFN)-Laboratori Nazionali di Frascati, Frascati, Italy, [6]Geology Department, Faculty of Science, Beni-Suef University, Beni suef, Egypt

Turbinaria ornata marine macro-algae (TUN) have been applied as carriers for the metallic zinc/ZnO blended nanoparticles, which were synthesized by implementing the extracted phytochemicals of the algae. The resulting hybrid bio-composite (Zn@ZnO/TUN) was characterized as a potential product of promising antioxidant and antidiabetic characteristics in synergetic studies. The obtained composite demonstrate t6he existing or complex biological active groups related to zinc (Zn-O stretching and tetrahedral Zn coordination) and organic groups (amino, methyl, carboxylic, alkynes, P=O, C–C–O, C=N, and N–O) corresponding to the extracted phytochemicals of algae (polysaccharides, phospholipids, lipids, fucose, and phosphodiester). The assessment of Zn@ZnO/TUN hybrid as an anti-oxidant agent validated excellent effectiveness towards the commonly examined radicals (DPPH (88.2 ± 1.44%), nitric oxide (92.7 ± 1.71%), ABTS (90.5 ± 1.8%), and $O_2^{\bullet-}$ (30.6 ± 1.32%), considering the determined performance for the commercially used standard (ascorbic acid). Regarding the antidiabetic properties, the incorporation of Zn@ZnO/TUN inhibits the function and activities of the key oxidizing enzymes, either the commercial forms (α-amylase (88.7 ± 1.3%), α-glucosidase (98.4 ± 1.3%), and amyloglucosidase (97.3 ± 1.4%) or the crude intestinal active forms (α-amylase (66.2 ± 1.4%) and α-glucosidase (95.1 ± 1.5%). This inhibitory effectiveness of Zn@ZnO/TUN is significantly better than the measured performances using commercialized miglitol drugs and slightly better than acarbose. Considering the expense and adverse effects of conventional medications, the synthesized Zn@ZnO/TUN blend could be evaluated as a marketable antidiabetic and antioxidant medication. The findings also demonstrate the influence of the derived phytochemicals from

Turbinaria ornata and the incorporation of its algae residuals as carriers for the metal nanoparticles on the biological function of the composite. The cytotoxicity investigation reflected safety effect of the composite on colorectal fibroblast cells (CCD-18Co) (96.3% cell viability) and inhibition effect on cancerous colorectal cells (HCT-116) (47.3% cell viability).

KEYWORDS

***Turbinaria ornata*, green synthesis, zinc, composite, antioxidant, antidiabetic**

1 Introduction

The sudden rise in diabetes prevalence, as reported globally in later periods, is one of the most important and urgent health concerns. Through 2030, the number of cases might exceed approximately 366 million, establishing it as the seventh leading cause of fatalities in the modern world (Arvanag et al., 2019; Behl et al., 2021; Billacura et al., 2022). Diabetes is a clinical illness affecting the pancreas and is categorized into two main types: (A) type-1 (T1-DM) and (B) type-2 (T2-DM), the latter being the most prevalent kind and is expected to comprise 90% of those diagnosed with diabetes around 2030 (Hsu et al., 2020; Behl et al., 2021). T2-DM is a severe metabolic condition characterized by an excessive production of reactive oxygen species (ROS) or oxidative radicals at excessive levels, as well as a rise in blood sugar levels after eating (post-prandial hyperglycemia) (Robkhob et al., 2020; Sagandira et al., 2021). Post-prandial hyperglycemia has emerged as the main risk factor for various clinical issues, including renal failure, cardiomyopathy, excessive hunger, death, excessive thirst, glucose in the urine, eye disease, and nerve damage (Hajra and Paul, 2018; Feldman et al., 2019; Dedvisitsakul and Watla-Iad, 2022). However, the production of reactive oxygen species (ROS) has crucial pathophysiological negative effects. Oxidative stress is associated with a clear decline in antioxidant activity, insulin intolerance, adverse effects on lipid peroxidation, and strong destruction of cell organelles and blood vessels (Asmat et al., 2016; Feldman et al., 2019; Robkhob et al., 2020; Kim et al., 2022).

The most frequently utilized commercially available and efficacious antidiabetic medications that have displayed significant reduction and control impacts on the concentrations of ROS along with post-prandial hyperglycemia include biguanides, acarbose, miglitol, a thiazolidinedione, sulfonylureas, and voglibose (Feldman et al., 2019; Robkhob et al., 2020). Regrettably, along with their high prices, the majority of the aforementioned medications have been associated with a number of health issues, including diarrhea, meteorism, abdominal distention, severe hypoglycemia, and hepatotoxicity (Yilmazer-Musa et al., 2012; Robkhob et al., 2020). As a result, in subsequent years, a variety of novel multifunctional materials containing a variety of biologically active chemical constituents have been established as probable strengthened antioxidant and diabetic medications. These compounds can also be used successfully as oxidative enzyme-inhibiting and scavenging agents (Robkhob et al., 2020; Malik et al., 2022). Among the evaluated chemically produced structures, CuO, ZnO, and NiO are examples of biologically active metal oxides that have demonstrated strong antidiabetic and antioxidant activities. Their distinct physicochemical characteristics (the exterior responsiveness along with surface area), inexpensive production costs, exceptional biological activities, notable biocompatibility, and elevated theranostic and therapeutic potential have been highlighted as reasons for their medical values (Singh et al., 2021; Malik et al., 2022; Velsankar et al., 2022).

The chemically produced nanoparticles of zinc oxide, along with their blended forms, have been widely used as biologically active compounds owing to their excellent anti-oxidant, biocompatibility, anti-diabetic, non-toxicity, and antitumor activities (Noohpisheh et al., 2020; Ansari et al., 2022; Velsankar et al., 2022). Zinc has been recognized as a chemical element that is essential to the functioning of the human body, particularly during the production of protein and nucleic acid (Singh et al., 2021; Ansari et al., 2022). The fabricated zinc oxides and their derivatives are widely utilized in various pharmaceutical, healthcare, and biological sectors. They serve as antioxidants, antimicrobial agents, chemotherapy drugs, and hypoglycemic agents. Furthermore, they are valuable components during the administration of drugs as carriers and in the tissue engineering sector (Singh et al., 2021; Sharma et al., 2022). The latest studies demonstrated that ZnO nanoparticles serve as beneficial antioxidants that can assist in controlling mitochondrial respiration and exhibit remarkable impacts on diminishing and hindering the activities of the oxidative enzymes and the generated ROS (Robkhob et al., 2020; Malik et al., 2022).

The aggregation tendencies of the fabricated ZnO nanoparticles triggered by van der Waals forces, along with their established superficial characteristics and fast recombination rates, have negative impacts on the production effectiveness of the free radicals and, consequently, the photocatalytic and biological performances (Saad et al., 2020; Malik et al., 2022). Furthermore, a number of investigations confirm that the fabrication method, manufacturing conditions, crystallite dimension, and geometry of

ZnO all have a major impact on the material's biological and medicinal properties (Yusof et al., 2019; Singh et al., 2021; Velsankar et al., 2022). Researchers have successfully specified various physical and chemical approaches to enhance the biological activity, genotoxicity, biocompatibility, antioxidant, and antibacterial qualities of ZnO. These methods include surface modifications and hybridization (Singh et al., 2021; Ansari et al., 2022; Shaaban et al., 2022). The modification approaches frequently used include (1) doping chemical-based ZnO with different transitional metal ions; (2) inserting ZnO across a suitable carrier or base; (3) combining fabricated ZnO with biodegradable biopolymers to produce composite materials; and (4) synthesizing chemical-based complexes involving ZnO and certain biologically active phytochemicals (Naureen et al., 2021; Ansari et al., 2022; Malik et al., 2022; Meer et al., 2022).

The interaction between zinc-based frameworks and phytochemical molecules, whether through the development of complexes or fabrication using plant or bioresource-mediated techniques, prompts their biological compatibility, antioxidant activities, and genotoxicity (Abdel Salam et al., 2022; Ansari et al., 2022; Meer et al., 2022; Prasad and Lall, 2022). As a result, the environmentally friendly production of zinc oxide employing bioresource botanical extracts composed of widely recognized phytochemicals as antioxidants, including sea algae, would have important beneficial diabetic effects. Green chemical synthesis approaches have attracted widespread attention over the past few decades due to their environmentally friendly, economically viable, effortless, harmless, bio-safe, and highly yielding nature for synthesizing non-agglomerated nanomaterials (Abukhadra et al., 2022; Velsankar et al., 2022). Furthermore, the particulates that develop frequently possess a layer consisting of vital phytochemicals that include alkaloids, proteins, phenolic molecules, amino acids, etc (Velsankar et al., 2022).

Additionally, earlier studies have shown that using inorganic and/or organic materials as base structures along with common macro- and micro-marine algae has a big positive effect on ZnO's chemical, physical, biological, and catalytic properties (Rabie et al., 2020; Saad et al., 2020). Recent studies have evaluated the biomass of algal species as a potential alternative bioresource, offering nutritional and medicinal advantages, facile cultivation, significant yields, and financial feasibility (El Shafay et al., 2016; Atugoda et al., 2021; Ahmed et al., 2022). They were frequently employed as an excellent supplier of a variety of essential biologically functioning chemicals that demonstrate remarkable antibiotic, anti-inflammatory, antifungal, antibacterial, antioxidant, and anti-tumor qualities (Khairy and El-Sheikh, 2015; El Shafay et al., 2016; Alreshidi et al., 2023). *Turbinaria* algae, a brown marine seaweed, is extensively found in tropical as well as subtropical areas, particularly the western Pacific, Indian Ocean, and Red Sea of Egypt, throughout various seasons (Bharath et al., 2021; Hasan et al., 2022; Pamungkas et al., 2024). *Turbinaria* possesses a variety of organic constituents, including terpenes, tannins, fucoxanthin, phenols, flavonoids, saponins, proteins, fucosterols, and sulfate carbohydrates. These chemicals display a wide range of practical applications, such as anticancer, antibacterial, antidiabetic, anti-ulcerative, antioxidant, and anti-inflammatory agents, in addition to their values in inhibiting cholesterol absorption (Maggio et al., 2022; Rosa et al., 2022; Elshikh and Al Farraj, 2024). The recent research on seaweed and its bioactive ingredients provides valuable insights into the development of potent anti-diabetic medications. Algae flourish in intricate ecosystems that provide quick adaptability to a variety of severe environmental factors, including temperature, salinity, nutrition, and ultraviolet (UV) fluctuations. As a consequence, algae develop a variety of biologically active compounds alongside secondary metabolic products exhibiting various biological functions to enable them to adapt to such conditions (De Morais et al., 2015; Hakim and Patel, 2020; Nguyen et al., 2024). The antioxidant properties of biologically active chemicals that occur naturally within the structure of these algae attracted the curiosity of scientists owing to the health care sector's interest in developing innovative chemicals possessing medicinal properties that can combat or mitigate diseases associated with oxidative stresses, including diabetes, atherosclerosis, cardiovascular problems, chronic inflammation, and malignancies (Lauritano et al., 2016; Mellouk et al., 2017; Ali et al., 2024).

As a result, using the *Turbinaria* framework as a support for green-developed ZnO and using phytochemicals extracted from algae as reducing or oxidizing agents could lead to new multifunctional hybrids with much better biological and pharmaceutical properties. There have been insufficient studies conducted to adequately address the biological significance and potential of employing green synthesized metallic zinc in blended form with ZnO nanoparticles and their chemical complexes with the extracted vital phytochemicals from coastal brown macro-algae (*Turbinaria ornata*) or hybrids with algae structure as substrate (Zn@ZnO/TUN). Consequently, this study tackles the biological activities of green-produced metallic zinc (Zn) for the first time, employing an extract from *Turbinaria* algae and its hybrid with the algae's structure as potent antidiabetic and antioxidant agents. This includes investigating the scavenging efficiency of commonly encountered oxidizing radicals using synthetically produced structures in synergetic manners, as well as their inhibitory impacts on the key enzymes.

2 Experimental work

2.1 Materials and chemicals

Zinc nitrate hexahydrate (Zn $(NO_3)_2$. $6H_2O$), which comes from Sigma Aldrich in Egypt and has a grade of 98%, is used as a chemical source in the production of green metallic zinc. We collected the brown marine macroalgae (*Turbinaria ornata*) (TUN) from the western coastal region extending from Quseir and Marsa-Alam in Egypt. These algae have been employed as a feedstock for the production of green solutions with reducing and oxidizing characteristics for effective production of health- and environmentally friendly metallic zinc, as well as a support for the produced zinc and ZnO nanoparticles. During the anti-oxidation and anti-diabetic tests, L-ascorbic acid, α-amylase, starch, 2,2`-azino-bis(3-ethylbenzothiazoline-6-sulphonic acid (ABTS), para-nitrophenylα-glucopyranoside (pNPG), α-glucosidase, and saline phosphate buffers were the most

10.3389/fmars.2024.1444618

important biological and chemical substances used (Sigma-Aldrich; Egypt).

2.2 Preparation of algal samples for extraction

After the collection process was finished along the coastline, the samples were transported to the laboratory. Algal species were identified according to (Botes, 2003) and (Guiry and Guiry, 2015). They underwent a thorough washing with seawater to eliminate sand and any other material that might have been attached to them. Then, they have been rinsed repeatedly with distilled water to get rid of any epiphytes or salts. Next, the algae had been dried in the shade either mechanically or using an electrical mixer until they turned into powder. The next step involved an additional drying stage at 50 °C for approximately 24 hours, which confirmed the successful and effective dehydration of the biological structure of TUN algae. Subsequently, the dehydrated had been extensively pulverized for an additional cycle into tiny particles using a standard household hand blender before being passed through a ball mill (Planetary Ball Mill PM 400) to get micro-fractions with particle sizes ranging from 50 to 190 µm. The resulting powder had been kept in a dark room and later subjected to various extraction, synthesis, and characterization techniques.

2.3 Synthesis of green Zn@ZnO/ TUN composite

2.3.1 Extraction of the phytochemicals form TUN algae

Prior to the synthesis procedures, the green extract solutions were derived from the algae structure as essential reducing and capping reagents during the production of the Zn nanoparticles in complexes with the TUN -based vital phytochemicals (Abukhadra et al., 2022). The obtained TUN micro-fractions (10 g) were first dispersed inside 100 mL of distilled water and stirred continuously at 700 rpm for 48 h in the presence of an ultrasonic generator (240 W) at a maintained temperature of 75 °C. The system was supplemented with 20 mL of methanol to enhance the liberation of the main phytochemicals, maintaining the mixing conditions for an additional 10 h. After that, the extracted phytochemicals as soluble chemicals in solution were isolated from the solid residual biomass of the TUN algae by filtration using Whitman filter paper. The methanolic extracts underwent initially phytochemical screening using Trease and Evans (1989) and Harborne (1973) reported techniques and the measured results were presented in Table 1.

TABLE 1 Qualitative estimation of the existed phytochemicals in the extract of TUN algae.

Content	TUN
Alkaloids	+
Tannins	-
Flavonoids	+
Glycosides	+
Saponins	-
Phenols	+
Terpenoids	+
Steroids	+

+ (Existed).
- (Absent).

2.3.2 Supporting of Zn@ZnO into TUN substrate

The remaining biomasses after the extraction stage as residuals or byproducts were washed extensively repeatedly for 5 cycles using distilled water, and each cycle continued for 10 minutes. This was followed by a drying step for 12 hours at 50 °C to be incorporated in the second synthesis process. The dried TUN biomass (5 g) was then pulverized within an aqueous solution of zinc nitrate (5 M; 100 mL) under complex mixing with a magnetic stirrer (700 rpm) and an ultrasonic generator (240 W). This was followed by the sudden incorporation of the previously prepared extracted TUN solutions (100 mL), and the mixture was homogenized by the same mixing system for an additional 24 hours at ambient temperature (30 °C) to ensure the successful precipitation of the green Zn and ZnO nanoparticles as decorated nanograins over the surfaces of TUN biomass. By the end of the synthesis step, the resulting composite (Zn@ZnO/TUN) was obtained by filtration, rinsed effectively using distilled water, and dried gently at 50 °C for 10 hours. Figure 1 showed a schematic representation of the synthesis processes. The green ZnO particles are frequently developed by a donor-acceptor process whenever zinc ions react with oxygen atoms originating from pytochemical compounds encountered in the algae-derived extracts (Abukhadra et al., 2022). The procedure consisted of three phases: (a) the activating phase, where Zn^{2+} ions were liberated out of their bearing salts; (b) the transformation of Zn^{2+} into a metallic state through the biofunctional groups existing throughout the obtained extract; (c) the oxidation of the metallic zinc to generate ZnO throughout the drying step; and (d) the stabilization of the resulting ZnO through further phyto-components within the extract (Abukhadra et al., 2022).

2.4 Characterization techniques

The crystalline forms and structural characteristics of each material have been evaluated by analyzing their X-ray diffraction patterns employing a PANalytical XRD diffractometer (Empyrean) equipped with a Cu-Kα radiation generator. The measurements have been performed within the range of 5° to 80°. The chemical structure was determined using the energy dispersive X-ray (EDX) technique, which analyzes the various elements based on their EDX spectra. The key chemical functionalities have been determined based on the FT-IR spectra of the examined ingredients using a Fourier transform infrared spectrometer (FTIR-8400S). The exterior features of the fabricated materials and their overall geometries have been assessed using SEM images acquired using a scanning electron microscope (Gemini-Zeiss, Ultra 55). The HRTEM photographs of synthetically produced products were used for examining and analyzing their internal characteristics

FIGURE 1
Schematic diagram for the synthesis of Zn@ZnO/TUN composite.

and blending procedures. The photos had been captured using a transmission electron microscope (JEOL-JEM, 2100). The surface area had been measured using a Beckman Coulter surface area analyzer (SA3100 type), based on the N_2 adsorption and desorption isotherm curves produced.

2.5 Antioxidant studies

2.5.1 Scavenging of nitric oxide radical

The scavenging qualities of the NOR radicals using commercial ZnO (C.ZnO), green ZnO by the extracted solution of the algae (T.ZnO), the ground fractions of the *Turbinaria* alga (TUN), ZnO/TUN, and Zn@ZnO/TUN composite have been tested implementing the method described by (Kitture et al., 2015). The ingredients were individually incorporated into sodium nitroprusside (2 mL; 10 mM) within buffering phosphate fluids of pH 7.4 (500 µL). The mixes underwent incubation individually at a specific temperature of 25 °C over a duration of 150 minutes. Following the incubation time frame, the solutions have been blended with diluent sulphanilic acid (500 µL; 1 M) before being cultivated for an additional brief duration of 5 minutes. Subsequently, the solutions had been diluted using naphthyl ethylenediamine dihydrochloride (0.1% w/v; 1 mL) and then incubated again over a further 30 minutes. In order to compute the scavenging percentage as described in Equation 1, the absorbance of the examined mixes was eventually measured using a microplate reader at 540 nm as compared to pure solutions lacking the assessed ingredients (controls).

$$Scavenging\ (\%) = \frac{A540_{Control} - A540_{Test}}{A540_{Control}} X\ 100 \qquad (1)$$

2.5.2 Scavenging of DPPH radical

The effectiveness of C.ZnO, T.ZnO, TUN, ZnO/TUN, and Zn@ZnO/TUN composites as DPPH radical scavengers has been determined using the antioxidant assessment that was successfully carried out by (Robkhob et al., 2020). The produced ingredients (100 µg/mL; 20 µL) had been individually incorporated into 80 µL of methanolic fluids that had been adequately supplemented by the analyzed DPPH radicals (100 µM) employing appropriate 96-well plates. The resulting blends were placed in incubators individually for 20 minutes with no source of light. By the completion of the incubation process, the absorbance levels of the examined mixes had been measured using a microplate reader at 517 nm with respect to the untested solutions lacking the evaluated products. The findings were subsequently employed to estimate the scavenging percentage using Equation 2.

$$Scavenging\ (\%) = \frac{A517_{Control} - A517_{Test}}{A517_{Control}} X\ 100 \qquad (2)$$

2.5.3 Scavenging of ABTS radical

Utilizing the scavenging test developed by (Dappula et al., 1273), the suitability of C.ZnO, T.ZnO, TUN, ZnO/TUN, and Zn@ZnO/TUN composites to be ABTS radical eliminators was assessed. The ABTS fluids implemented throughout the assays have been generated by dissolving the ABTS component (44 mg) in 10 mL of deionized water. Subsequently, these buffers were individually reinforced using $K_2S_2O_8$ (3 mM) as an important ingredient to produce the unbound cations ($ABTS^{\bullet+}$) that comprise the ABTS radicals. The whole process had been carried out under dark conditions at a controlled temperature of 25°C for a duration of 18 hours. At the final stage of this procedure, the resulting systems were diluted with alcohol at a ratio of 1:29 to

generate newly formed $ABTS^{\bullet+}$. Following the above-mentioned procedures, all of the synthesized ingredients had been combined individually (at a concentration of 100 µg/mL) with the ABTS solutions that had been generated earlier (at a volume of 290 µL). The resulting blends then underwent incubation for a duration of 30 minutes. The absorbance levels resulting from the examined mixes were measured using a microplate reader at 734 nm, in contrast to the untreated fluids lacking the investigated components (controls). The obtained values were then used to compute the scavenging percentage, as described in Equation 3.

$$Scavenging\ (\%) = \frac{A734_{Control} - A734_{Test}}{A734_{Control}} X\ 100 \quad (3)$$

2.5.4 Scavenging of superoxide radical

Utilizing the scavenging experiment developed by (Robkhob et al., 2020), the possible applications of C.ZnO, T.ZnO, TUN, ZnO/TUN, and Zn@ZnO/TUN as antioxidants against the super oxide radicals ($O^{\bullet-}$) were assessed. The produced ingredients (100 µL) had been individually combined with pre-made mixes containing EDTA (200 µL; 12 mM), NBT (100 µL; 0.1 mg), riboflavin (100 µL; 20 µg), and ethanol (200 µL). Following a 5-minute exposure to an illumination provider, the outcomes of the preceding blending processes were complemented individually with 3 mL of phosphate-based buffers. Then, using a microplate reader set to 540 nm, the absorbances corresponding to the examined mixes were tracked in relation to the untreated fluids with the materials (controls). The data were then used to compute the scavenging percentage using Equation 4.

$$Scavenging\ (\%) = \frac{A540_{Control} - A540_{Test}}{A540_{Control}} X\ 100 \quad (4)$$

2.6 Anti-diabetic studies

2.6.1 Inhibition assay of porcine pancreatic α-amylase

The effectiveness of C.ZnO, T.ZnO, TUN, ZnO/TUN, and Zn@ZnO/TUN as inhibitor compounds towards the frequently employed commercialized pancreatic α-amylase enzymes has been investigated by implementing the inhibitory assays by (Robkhob et al., 2020). The ingredients were combined individually with the α-amylase enzymes at a specific concentration (100 µg/mL and 50 µg/mL, respectively). The resulting mixtures were then incubated for 10 minutes at a temperature of 37 °C. Subsequently, the apparatus was enriched by administering a starch substrate at a concentration of 1%. The absorbance levels were thereafter measured using a microplate reader at 540 nm with respect to the untreated fluids lacking the materials being investigated (controls). The outcomes established were used to estimate the percentage of inhibition using Equation 5.

$$Inhibition\ (\%) = \frac{A540_{Control} - A540_{Test}}{A540_{Control}} X\ 100 \quad (5)$$

2.6.2 Inhibition assay of crude murine pancreatic α-amylase

This experiment was conducted to determine the efficacy of C.ZnO, T.ZnO, TUN, ZnO/TUN, and Zn@ZnO/TUN in inhibiting the crude effective enzymes as compared to the marketed enzymes studied. The pancreatic enzyme has been obtained through the pancreas of a male Swiss mouse approximately 10 weeks of age. The pancreas under investigation was treated through a 12-hour period of fasting. Next, the starved pancreas had been surgically extracted and submerged delicately within a phosphate-based buffered solution that included inhibitors of protease. Subsequently, the supernatant-deficient cells had been eliminated using a rapid centrifugation procedure (15 min; 10000 rpm). The apparatus was subsequently diluted systematically until the microplate reader (240 nm) detected 0.4 as absorbance. Under such situations, the pancreas could potentially be employed as a supplier of functional crude enzymes. The inhibiting examination of synthesized ingredients towards the enzyme was then conducted using the identical protocols outlined in Section 2.5.1.

2.6.3 Inhibition assay of α-glucosidase

The efficacy of C.ZnO, T.ZnO, TUN, ZnO/TUN, and Zn@ZnO/TUN as inhibitor agents towards the commercially available version of α-Glucosidase enzymes was assessed using the inhibitory experiments developed by (Sanap et al., 2010). The derived ingredients had been individually combined with the examined α-glucosidase enzymes at a specific concentration (100 µg/mL and 100 µL; 0.1 unit/mL, respectively). The resultant mixtures were then incubated for 60 minutes at a temperature of 37°C. Subsequently, the apparatus was further enriched by adding a pNPG solution (10 mL) prior to being re-incubated for a further 10 minutes. Afterwards, 2 mL of Na_2CO_3 solution with a concentration of 0.1 M was introduced into each apparatus individually in order to immediately stop the ongoing processes. The absorbance levels of the released nitrophenol from pNPG had been measured using a microplate reader at 420 nm with respect to the untreated fluids lacking the compounds being studied (controls). The findings obtained were then used to estimate the inhibitory percentage, as described in Equation 6.

$$Inhibition\ (\%) = \frac{A420_{Control} - A420_{Test}}{A420_{Control}} X\ 100 \quad (6)$$

2.6.4 Inhibition assay of crude murine intestinal α-glucosidase

The natural intestinal α-glucosidase enzymes had been obtained using the approach that was outlined earlier throughout the separation of the raw α-amylase enzymes in the specified section.2.5.2. Inhibiting experiments of C.ZnO, T.ZnO, TUN, ZnO/TUN, and Zn@ZnO/TUN towards the crude intestinal α-glucosidase enzymes had been performed using identical protocols as those described for inhibiting the commercially available enzymes in the previous section.2.5.3 The potential involvement of p-nitrophenyl-α-D-glucopyranoside as a base is being considered.

2.6.5 Amyloglucosidase inhibition assay

C.ZnO, T.ZnO, TUN, ZnO/TUN, and Zn@ZnO/TUN were tested for their suitability as amyloglucosidase-inhibiting agents using the inhibitory assay described by (Lawande et al., 2017). The ingredients were combined individually with the amyloglucosidase enzymes at a specific concentration (100 µg/mL) and enzyme load of 0.1 unit/mL. The resultant mixtures were then incubated at 37 °C for 10 minutes in the presence of 1% starch substrates. Subsequently, the mixtures' absorbance levels had been measured using a microplate reader at 540 nm in relation to untreated solutions devoid of the investigated components (controls). The inhibiting percentage was then computed using the formula in Equation 5.

2.7 Cytotoxicity properties

The cytotoxicity of Zn@ZnO/TUN had been determined by measuring its effect against normal colorectal fibroblast cells (CCD-18Co) and cancerous colorectal cells (HCT-116). The cell lines underwent cultivation in Dulbecco's Modified Eagle Media enriched in 10% fetal bovine serum, 100 µg/mL of penicillin, and 100 µg/mL of streptomycin. The cells underwent incubation at a temperature of 37°C containing a 5% concentration of CO_2 in a completely humidified atmosphere. The Y79 cells went through cultivation and were distributed into 96-well plates at a density of about 1×10^6 cells per well. The cells then underwent incubation for 24 hours in order to conduct cytotoxic assessment utilizing the 3-(4, 5-dimethyl-2-thiazolyl)-2, 5-diphenyl-tetrazolium bromide (MTT) test. Different doses of Zn@ZnO/TUN in a solution of 0.1% DMSO were incorporated and underwent incubation for 24 hours within an incubator with an atmosphere of 95% air and 5% CO_2. Following incubation, 10 µl of MTT solution (5 mg/mL in PBS) was introduced into each well and placed in the incubator for 4 hours at a temperature of 37°C. The formazan that was produced was dissolved in 100 µL of DMSO, and the number of live cells was determined by measuring the absorbance at 570 nm. The impact of the structure on the growth of Y79 cells was quantified as the percentage of cell viability, determined by applying Equation 7.

$$Cell\ \ viability\ \ \% = \frac{\text{A 750 of treated cell}}{A\ \ 750\ \ of\ \ control\ \ cell} \times 100 \qquad (7)$$

2.8 Statistical analysis

The reported data have been included in their mean values ± the established standard errors for these mean data (S.E.M.), assuming the n value equals 3. The significance and accuracy of the statistical tests for the outcomes depend on the pairing tests and analyses of variance (ANOVA), where *P levels are less than 0.05.

3 Results and discussion

3.1 Characterization of the synthetic structures

The obtained XRD patterns of the incorporated algal structure of *Turbinaria ornata* as substrate, in addition to its residual biomass after treatment and extraction processes, as well as the obtained Zn@ZnO/TUN composite, are presented in Figure 2. The recognized pattern of the algae as the raw precursor exhibits the common broad peak of the amorphous organic materials (a round 2 Theta angle of 22°), in addition to several peaks that might be related to the associated impurities and salts (Figure 2A). Regarding the recognized pattern after the washing and extraction steps, the observed patterns demonstrate strong reductions of the previously identified peaks corresponding to the associated impurities of salts. Furthermore, the pattern clearly reveals the amorphous nature of the organic carbonaceous structures of the resulting biomass after the extraction procedures (Figure 2B). The synthesized Zn@ZnO/TUN composite's recognized pattern, characterized by a remarkable, very broad peak or hump, clearly demonstrates the amorphous nature of the incorporated TUN biomasses (Figure 2C). Moreover, the existence of the decorated green metallic zinc in blend with ZnO as crystalline phases was confirmed by detecting their corresponding peaks. The existence of ZnO as hexagonal wurtzite was confirmed by its detectable

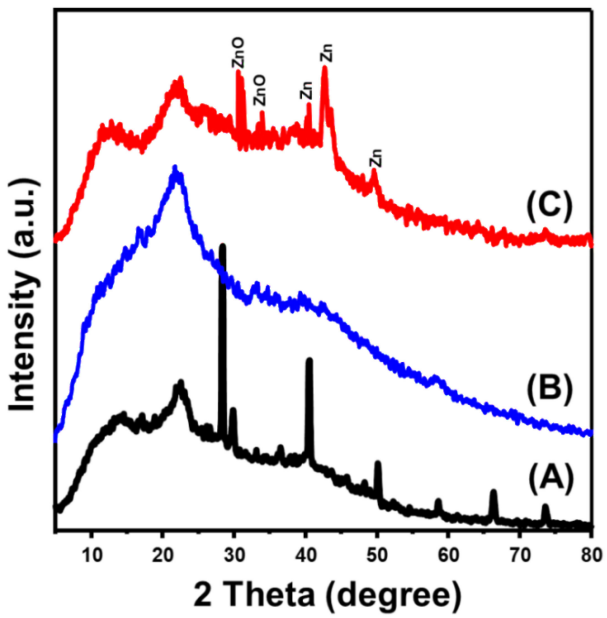

FIGURE 2
XRD patterns of *Turbinaria ornata* algae (TUN) **(A)**, residuals of TUN after extraction **(B)**, and synthetic Zn@ZnO/TUN composite **(C)**.

characteristic peaks around 31.8° (100), 34.4° (002), and 36.7°(101) (JCPDS no. 65–3411; JCPDS no. 36–1451) (Figure 2C). For the blended metallic zinc as separated crystalline phase, it was confirmed by the observable peaks at 39.03° (100), 43.24° (101), and 54.36° (102) (PDF. card: 04–0831; JCPDS 36–1451; JCPDS no. 00–004-0784) (Figure 2C). The average crystallite size of formed ZnO phase was determined according to the Debye-Scherer formula to be 4.2 nm while the detected average crystallite size of the blended Zn metal is 8.4 nm.

The previous findings also relied on the FT-IR spectrum of the synthetic materials, which was compared to the spectrum obtained from the algal structure of *Turbinaria ornata* (Figure 3). The mean chemical groups derive from proteins, lipids, and polysaccharides that are found in the algal cell wall. The cell wall contains a variety of chemical groups, which include carboxyl (found in fatty acids along with amino acids), hydroxyl (found in polysaccharides), phosphate, amine, and sulfonate (Dmytryk et al., 2014). The broad band around 3409 cm^{-1} indicates the stretching vibration of O-H bonds within the existed the amine groups or the structures of polysaccharides (Figure 3A) (Fauziee et al., 2021; Fawzy et al., 2022). The spectrum also reflected the remarkable detection of the corresponding bands of the C-H bonds that signifies the carboxylic groups of the existed phospholipids and lipids within the structure of TUN biomass, pyranoid rings, and C6 groups of fucose (2927 cm^{-1}) (Palanisamy et al., 2017; Dulla et al., 2018; Fauziee et al., 2021). Carboxylic along with amino groups constitute 70% of the structural components within the cell walls of the majority of brown algae. These compounds play a crucial role in facilitating the binding of metallic ions (Fawzy et al., 2022). The marked bands around 1630 cm^{-1}, 1529 cm^{-1}, and 1430 cm^{-1} signifies the stretching of C=N, N–O stretch-nitro compounds, bending of CH2 alongside CH3 within the methyl groups (Itroutwar et al., 2019; Fawzy et al., 2022). The detectable band around 1266 cm^{-1} can be assigned to the stretching of C–C–O or phosphodiester P=O corresponding to the existed protein (Fawzy and Gomaa, 2020). Moreover, the identified band at 1038 cm^{-1} declared the existence of primary alcohol by signifying the stretching vibration of its C-OH bond (Raj et al., 2023). Also, the detectable bands at 818 cm^{-1} and 687 cm^{-1} donate C=H bending-alkenes and –C=C– stretch alkynes, respectively (Itroutwar et al., 2019).

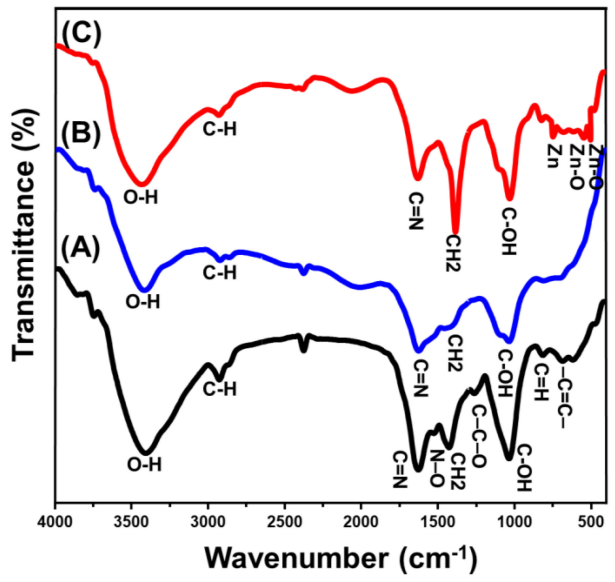

FIGURE 3
FT-IR spectra of algal structure of *Turbinaria ornata* algae **(A)**, the algal structure after the extraction process **(B)**, and synthetic Zn@ZnO/TUN composite **(C)**.

After the extraction procedures, the obtained FT-IR spectrum retains the same characteristic bands reported for the raw algae's chemical structure (Figure 3B). However, these bands exhibit a remarkable declination in their intensities, along with observable fluctuations in their positions. This indicates the impact of the washing and extraction processes on the algae's chemical structure, as they leach some of its vital phytochemical compounds. Regarding the Zn@ZnO/TUN composite's spectrum, there is also clear detection for the declination in the intensities of the common bands corresponding to the functional structure of the algae, reflecting a significant interaction effect for the loaded zinc particles (Figure 3C). The newly detected bands with considerable intensities around 822 cm^{-1}, 546 cm^{-1}, and 478 cm^{-1} signified the coordination of tetrahedral Zn, ZnO stretching, and Zn-O stretching, respectively (da Silva-Neto et al., 2019; Yang et al., 2022). The reported findings from the FT-IR analysis are strongly consistent with the results obtained from the EDX spectrum and elemental composition (Figure 4). The EDX spectrum of Zn@ZnO/TUN clearly demonstrated the presence of zinc as a crucial component in the composite, alongside the algal structure serving as the substrate, represented by the C element (Figure 4).

The morphological studies were performed based on the SEM images of the natural TUN algae, the residuals of the algae after the washing and extraction procedures, and the green supporting of Zn@ZnO nanoparticles (Figure 5). The recognized particles of the algae prior to any modification display the commonly reported geometries for algal structure as massive and compacted particles with no definite outlines (Figure 5A). High magnification images of the algae structure's surface reveal its irregular topography, which includes exposed and partially tortuous sections, as well as the detection of cellular network structure (Figure 5A). These features can significantly enhance the interacting interface and surface area. The extraction procedures resulted in a remarkable impact on the previously described surficial morphologies of the algae, in addition to the considerable detection of intersected blended plates forming observable porous framework that might indicate stripping for the main component of the algae or considerable separation of other species of polysaccharides (Figures 5B, C). The obtained SEM images of the Zn@ZnO/TUN composite reflected the extensive existence of the zinc particles as nanograins (Figure 5E). These zinc nano-grains appeared as coating layers over the algae's surface, and their development over the algal biomass resulted in numerous interstitial nano-pores, giving the composite porous properties and a higher surface area per volume (Figures 5D–F).

The previously mentioned geometries had a significant impact on the calculated surface area as well as the particle size distribution. With the different modification procedures, the measured surface area shows

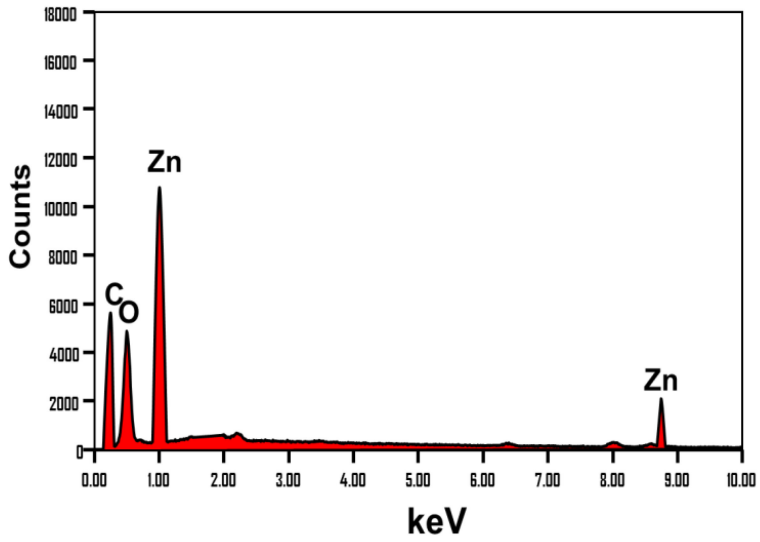

FIGURE 4
EDX spectrum of the synthesized Zn@ZnO/TUN composite.

a noticeable increase. The starting TUN exhibits a surface area of 6.2 m^2/g, and this value increased to 8.3 m^2/g after the washing and extraction steps. The calculated value for Zn@ZnO/TUN increased significantly, reaching 16.4 m^2/g. This reflects the impact of the crystallite size of the zinc nanoparticles and the interstitial nanopores on the textural qualities of the resulting composite. The synthetic Zn@ZnO/TUN particulates display narrow particles size distribution properties ranged from 293 nm up to 312 nm and the majority exhibit particle size around 300 nm (Supplementary Figure S1).

3.2 Antioxidant properties

3.2.1 Nitric oxide scavenging

The production of reactive oxygen species (ROS) throughout aerobic respiration, along with electron transportation pathways, leads to significant oxidative damage and several degenerative illnesses (Dhall and Self, 2018). Regarding these reactive species, the inconsistent formation of volatile free nitric oxide radicals (NOR) is having some serious drawbacks, including DNA

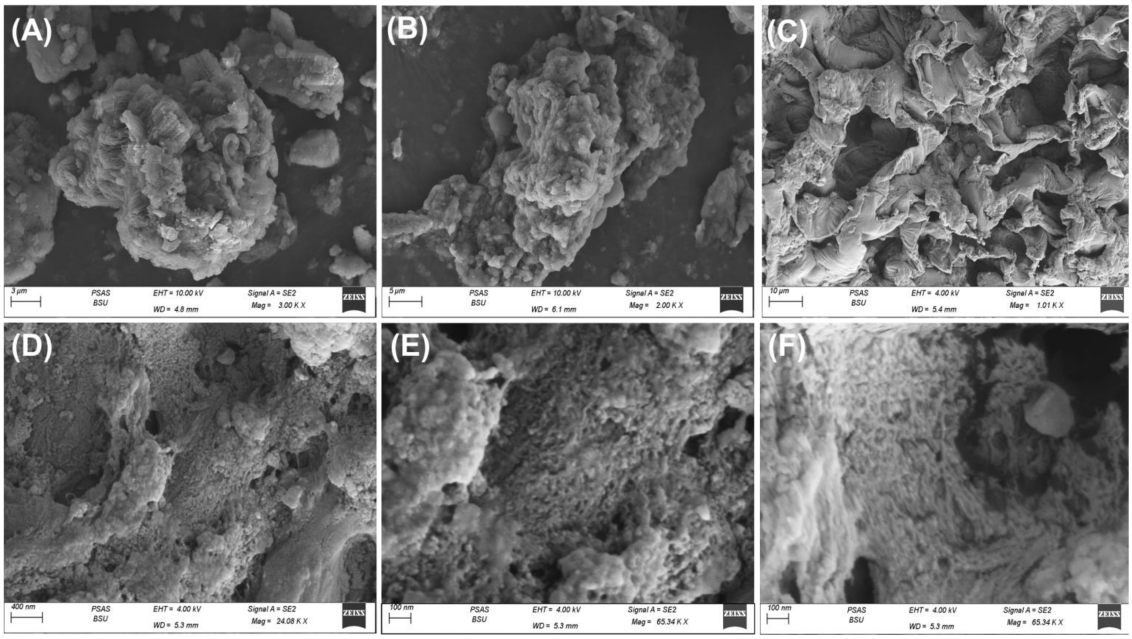

FIGURE 5
SEM images of natural TUN algae **(A, B)**, the algal structure after the washing and extraction steps **(C, D)**, and the synthesized Zn@ZnO/TUN composite showing the supporting zinc nanoparticles **(E, F)**.

breakage, cellular cytotoxicity, and neurons dying (Sharpe et al., 2011; Parul et al., 2013; Robkhob et al., 2020). The metal oxides usually evaluated as beneficial antioxidants exhibited notable scavenging powers for NOR. The scavenging performance of ZnO towards NOR significantly increased following the implementation of the integration of metallic Zn and the incorporation of TUN particulates as a support (Figure 6A). The scavenging% of NOR as determined by TUN, commercialized ZnO (C.ZnO), and green-produced ZnO utilizing the TUN-extracted chemicals (T.ZnO) were 26.3 ± 1.64, 35.7 ± 1.57%, and 39.8 ± 1.12, respectively (Figure 6A). Hence, the integration of TUN-extracted phytochemical-rich solutions throughout the "green" production procedure enhances the antioxidant properties of T.ZnO against NOR by about 4% as compared to C.ZnO. These findings align with the outcomes published in earlier studies (Figure 6A) (Song et al., 2022). This may be attributed to the controlled dimensions of the ZnO crystals and their non-agglomerated characteristics. Furthermore, the metallic oxides synthesized using these techniques frequently develop a complex with the essential botanical compounds present in the applied extract that serve as reduction ingredients, resulting in the formation of a fine capping layer across the outermost layer of the metallic oxides. This often triggers the biological functions of the metallic oxides, in addition to their scavenging or capturing performances, particularly towards NOR.

The insertion of the TUN support to generate the ZnO/TUN and Zn@ZnO/TUN hybrids leads to a significant increase in the NOR capturing or trapping function, reaching 63.4 ± 1.45% and 92.7 ± 1.71% (Figure 6A). The observed behaviors of ZnO/TUN and Zn@ZnO/TUN exhibit a notable increase compared to the actions of unbound TUN, C.ZnO, and T.ZnO. The beneficial effects of the TUN base material on the exposed and interfacing surfaces of the supported zinc particles, together with its lowering influence on the accumulation affinities associated with the loaded particulates, were attributed to the enhancing influence that has been identified (Robkhob et al., 2020). Additionally, it has been revealed that chemical ingredients belonging to TUN, a coastal brown macroalgae, have significant antioxidant properties. This leads to increased rates of contact with liberated reactive oxidative species (Rudayni et al., 2023). Also, the higher performance of Zn@ZnO/TUN as compared to ZnO/TUN might be assigned to the existed surficial electrons across the interfaces of Zn@ZnO which pair successfully with the lone pairs of OH free radicals (Rabie et al., 2020; Song et al., 2022). It was proved that the electron-supplying efficiency display strong controlling effect on the antioxidant activities of investigated metal oxides. Therefore, the integration between metallic zinc and ZnO in green blend enhances effectively the production rates and quantities of surficial electrons and in turns the scavenging properties of the free radicals. Hence, the synthesized Zn@ZnO/TUN hybrid has superior antioxidant

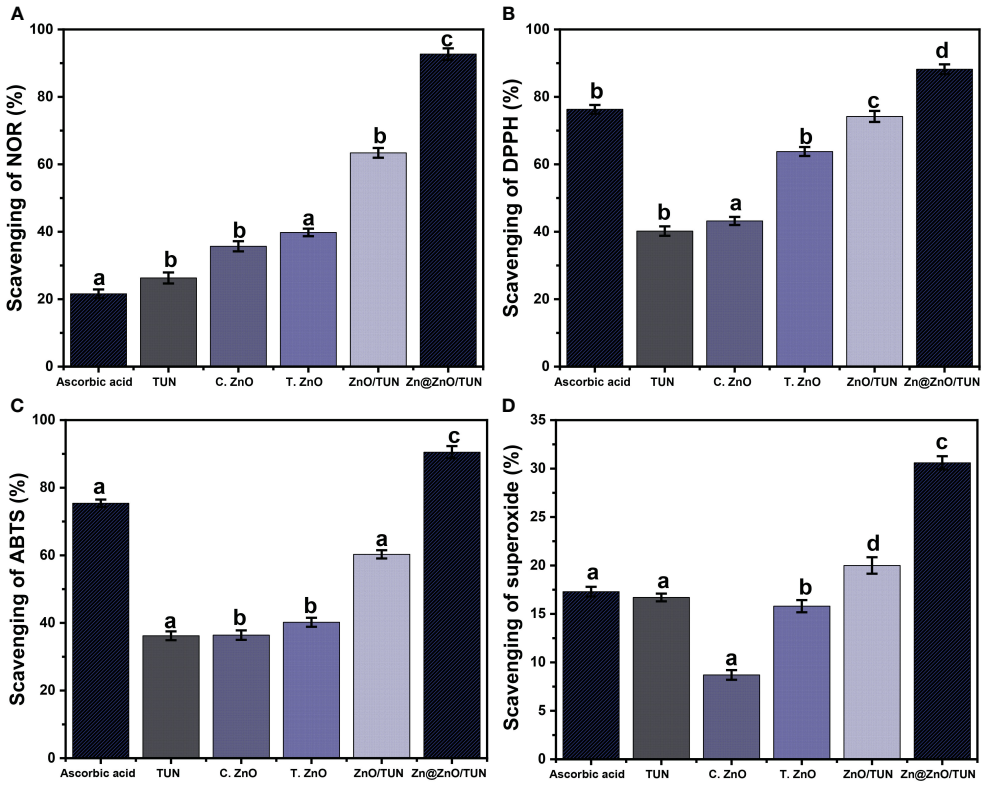

FIGURE 6
The antioxidant performances of TUN, C.ZnO, T.ZnO, ZnO/TUN, and Zn@ZnO/TUN structures against **(A)** Nitric oxide; **(B)** DPPH; **(C)** ABTS; and **(D)** super oxide radicals. The values are the averages of 5 replicates, the error bars indicate the standard error of means, and different letters specify a statistical difference between the means (P<0.05).

properties neither toward NOR in contrast to the individual ZnO, TUN, and ZnO/TUN components, alongside the commercially applied ascorbic acid as a reference (21.6 ± 1.33%) (Figure 6A).

3.2.2 DPPH radical scavenging

Synergistic experiments have evaluated the DPPH-scavenging efficiency of Zn@ZnO/TUN, comparing it with TUN, C.ZnO, T.ZnO, and ZnO/TUN. The described characteristics closely correspond to the observable aspects throughout the scavenging activities of NOR (Figure 6B). The scavenging % achieved utilizing Zn@ZnO/TUN is 88.2 ± 1.44%, and this is significantly greater than the level of effectiveness noticed for each separate ingredient (Figure 6B). The establishment of zinc as metallic particles in composite with ZnO combined with the insertion of the TUN support greatly boosted the scavenging performances of zinc-dependent structures alongside the algal functional groups to eliminate the DPPH radical. Therefore, the reported performance of the composite is considerably greater than the effectiveness of ascorbic acid as a commercially used standard (76.3 ± 1.28%) (Figure 6B). The previously declared findings rely on the realized behaviors reported for TUN (40.2 ± 1.4%), C.ZnO (41.7 ± 1.58%), T.ZnO (63.8 ± 1.33%), and ZnO/TUN (74.2 ± 1.63%) (Figure 6B). The sequestration process of DPPH radicals through the exteriors of synthesized metals and metal oxides involves electron (e^-) and proton (H^+) transfer processes targeting the organic structures of DPPH radicals (Dappula et al., 1273; Rudayni et al., 2023). The improved charge separation effectiveness of metal-based frameworks may boost their performance throughout the scavenging processes. The inserted metallic zinc in blend with ZnO enhances the production rates of the surficial electrons alongside the charge separation effectiveness which in turns improve the activity of Zn@ZnO in comparison with ZnO. Also, presence of numerous negatively charged chemical groups within the TUN structure may expedite the charge separation events, alongside the algal substrate's ability to enhance the interacting surfaces across the DPPH radicals and the biologically active zinc nanostructures (Liu et al., 2017).

3.2.3 ABTS radical scavenging

The scavenging assays of ABTS were extensively studied as a reliable measure of the antioxidant capacity of synthetically produced materials, particularly blends or hybridized frameworks. These experiments assess the decrease in the content of the released ABTS cationic radicals ($ABTS^{\bullet+}$), which indicates the antioxidant qualities of the materials being tested. Synthetically manufactured nanostructures with efficient hydrogen-donating antioxidant processes can potentially be used as successful scavengers to eliminate the $ABTS^{\bullet+}$ radicals. As a result, synthesized metals and metal oxides, whether in their pure state or modified by hybridizing with an appropriate support or carrier, are strongly recommended as effective scavengers against $ABTS^{\bullet+}$. The $ABTS^{\bullet+}$ scavenge% encountered for TUN (36.2 ± 1.3%), C.ZnO (36.4 ± 1.45%), T.ZnO (40.2 ± 1.34%), and ZnO/TUN (60.3 ± 1.22%) were considerably less than the value that was determined for the ascorbic acid as the implemented control (75.4 ± 1.14%) (Figure 6C). The incorporation of metallic zinc/ZnO nanoparticles, produced using environmentally friendly methods, directly into the TUN matrix along with important bioactive phytochemicals derived from algae (Zn@ZnO/TUN), led to a substantial increase in its ability to scavenge $ABTS^{\bullet+}$ radicals, reaching a level of 90.5 ± 1.8%. This activity was considerably greater than that of ascorbic acid, as shown in Figure 6C.

3.2.4 Superoxide radical scavenging

The superoxide anions ($O_2^{\bullet-}$) are a type of chemically active oxygen radical that are frequently produced inside cellular organelles, including mitochondria. It rapidly converts into different oxidative species that include hydroxyl radicals ($^{\bullet}OH$) in addition to H_2O_2. The spontaneous production of $O_2^{\bullet-}$ along with its altered forms leads to serious physiological disorders and poses multiple threats to health, involving the degradation of DNA, RNA, and proteins and eventually the development of degenerative illnesses (Hamasaki et al., 2008; Xie et al., 2018). It is generally thought that the human body has built-in defenses against released oxygen and its byproducts, as well as the oxidizing stresses that come from them. These mechanisms are crucial for maintaining stable physiological homeostasis. Nevertheless, different disorders negatively impact the physiological reactions of human beings throughout the process of generating defensive mechanisms, either in terms of the kind or the necessary amounts needed to counteract the concentrations of the released radicals. Consequently, it is highly advised to use distinctive and biocompatible nanostructures for efficient removal of $O_2^{\bullet-}$. The scavenging performance of $O_2^{\bullet-}$ by TUN (16.7 ± 1.11%), C.ZnO (8.7 ± 1.16%), and T.ZnO (15.8 ± 1.43%) is significantly lower than that of the ascorbic acid as the incorporated control (17.3 ± 1.34%) (Figure 6D). However, the antioxidant capacity of and ZnO/TUN (20 ± 1.65%) and Zn@ZnO/TUN (30.6 ± 1.32%) is much greater than that of the frequently employed ascorbic acid, as shown in Figure 6D.

3.3 Antidiabetic properties

3.3.1 Porcine pancreatic α-amylase inhibition assay

The anti-diabetic behaviors of TUN, C.ZnO, T.ZnO, ZnO/TUN, and Zn@ZnO/TUN were evaluated using synergistic experiments focusing on the inhibitory impacts on the α-amylase enzymes. The α-amylase enzyme is a crucial and predominant enzyme for digestion that effectively disintegrates complicated carbohydrate molecules, like starch, into less complicated types, including maltose, that quickly converts to sugar (Robkhob et al., 2020). Hence, synthesized nanomaterials that exhibit notable and rapid inhibitory properties towards the α-amylase digestive enzyme will ultimately lead to a substantial reduction in the degradation and disintegration levels of complicated sugars. Consequently, this will ultimately result in diminished absorption effectiveness of dietary carbohydrates and decreased quantities of blood glucose (Shu et al., 2023). As a result, diabetes-related post-meal hyperglycemia may be

effectively managed at notable and secure thresholds (Meer et al., 2022). The inhibiting % of the α-amylase enzyme using Zn@ZnO/TUN (88.7 ± 1.3%) shows significant antidiabetic action in comparison with the common commercially accessible medications, acarbose (75.2 ± 1.68%) as well as miglitol (18.3 ± 1.42%) (Figure 7A). The synthesized T.ZnO (51.8 ± 1.3%) and ZnO/TUN (73.4 ± 1.5%) showed greater inhibitory impacts on the α-amylase enzymes in contrast to TUN (41.2 ± 1.8%) and C.ZnO (40.3 ± 1.6%) in addition to miglitol medication (18.3 ± 1.42%) (Figure 7A). The detectable improvement in the antidiabetic effectiveness of the synthesized ZnO and Zn/ZnO blend may be attributed to the presence of the capping layer that formed through the phytochemicals extracted from algae and the incorporation of the TUN support. The implementation of the TUN support significantly decreased the tendency of synthesized nanoparticles to clump together, hence increasing their interactions and exposure to enzymes across their exteriors (Deng et al., 2022; Malik et al., 2022; Song et al., 2022; Shu et al., 2023). The clustering and accumulation of metals and metal oxides have a negative impact on their biological functions and their potential to hinder oxidizing enzymes (Yang et al., 2022). In comparison to costly commercially available medications that frequently have undesirable effects, Zn@ZnO/TUN can be suggested as a possible strengthened, affordable, successful, and reliable antidiabetic agent, depending on its inhibitory effects on the porcine pancreatic α-amylase enzyme (Rehana et al., 2017; Vinotha et al., 2019).

3.3.2 Murine pancreatic α-amylase inhibition

The inhibitory effects of TUN, C.ZnO, T.ZnO, ZnO/TUN, and Zn@ZnO/TUN on the function of the murine pancreatic α-amylase enzyme have been evaluated to determine their capacity to suppress the functions of metabolically primitive living enzymes. The inhibiting experiments were conducted using a synergistic approach, implementing the influence of green fabrication procedures and integrated TUN support. The synthesized Zn@ZnO/TUN blend effectively reduces the activity levels of the α-amylase enzyme (in its crude activated form) by 66.2 ± 1.4%. This investigation reveals the better antidiabetic effects of the tested composite (Zn@ZnO/TUN) in comparison to acarbose (61.4 ± 1.55%) along with miglitol (11.2 ± 1.61%), which are routinely prescribed commercialized medicines and employed as standards (Figure 7B). The synthesized ZnO/TUN (56.8 ± 1.9%) showed stronger inhibitory impacts on the α-amylase enzyme than TUN (13.4 ± 1.2%), C.ZnO (9.8 ± 1.12%), and T.ZnO (14.3 ± 1.53%) alongside the miglitol medication (18.3 ± 1.42%) (Figure 7B). The study's outcomes demonstrated the great potential of Zn/CSR as powerful and efficient antidiabetic drugs towards both the commercially available α-amylase enzyme and the biologically active enzyme.

3.3.3 Pancreatic α-glucosidase inhibition

The inhibitory impacts of TUN, C.ZnO, T.ZnO, ZnO/TUN, and Zn@ZnO/TUN on the α-glucosidase enzyme have been investigated in order to regulate its activity as a crucial and highly efficient enzyme involved in the metabolic processes of dietary starches and polysaccharides. Consequently, the generation of potent inhibitors targeting the α-glucosidase enzymes may effectively modulate and manage the digestion of glucose molecules within the bloodstream, leading to a significant reduction in hyperglycemia (Velsankar et al., 2022). The blend of Zn@ZnO/TUN exhibited a high inhibitory activity (98.4 ± 1.3%) with respect to the pancreatic α-glucosidase enzymes, indicating that it might function as an anti-diabetic agent. This efficacy was assessed in comparison with that of miglitol (90.2 ± 1.31%) and acarbose (96.4 ± 1.45%), together with the individual phases of TUN, C.ZnO, T.ZnO, and ZnO/TUN (Figure 8A). T.ZnO (75.8 ± 1.5%) and ZnO/TUN (94.3 ± 1.8%) have stronger inhibiting properties than TUN (41.6 ± 1.3%) and C.ZnO (38.2 ± 1.2%) (Figure 8A). The observed responses align with the findings in the existing literature regarding the combined impact of transitional metals complexing with vital phytochemicals and the use of appropriate supports on the biological activities of ZnO and zinc metallic nanoparticles. These nanoparticles have demonstrated potential as both antioxidants and antidiabetic agents.

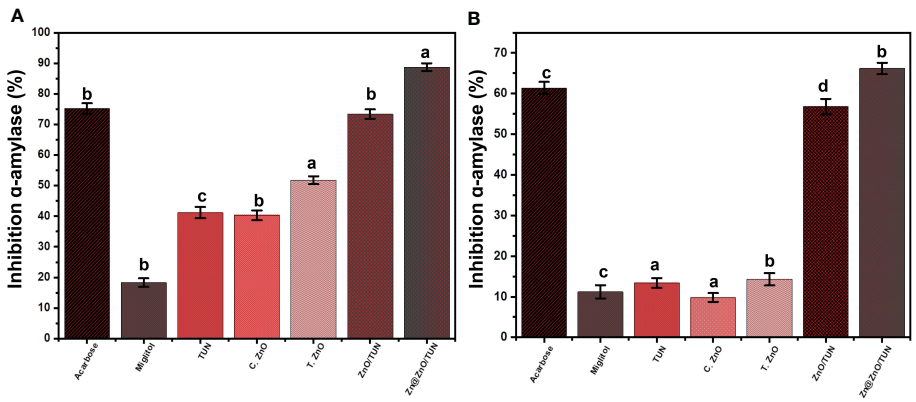

FIGURE 7
The inhibition properties of TUN, C.ZnO, T.ZnO, ZnO/TUN, and Zn@ZnO/TUN structures against Porcine pancreatic **(A)** and Murine pancreatic **(B)** α-amylase enzyme. The values are the averages of 5 replicates, the error bars indicate the standard error of means, and different letters specify a statistical difference between the means (P<0.05).

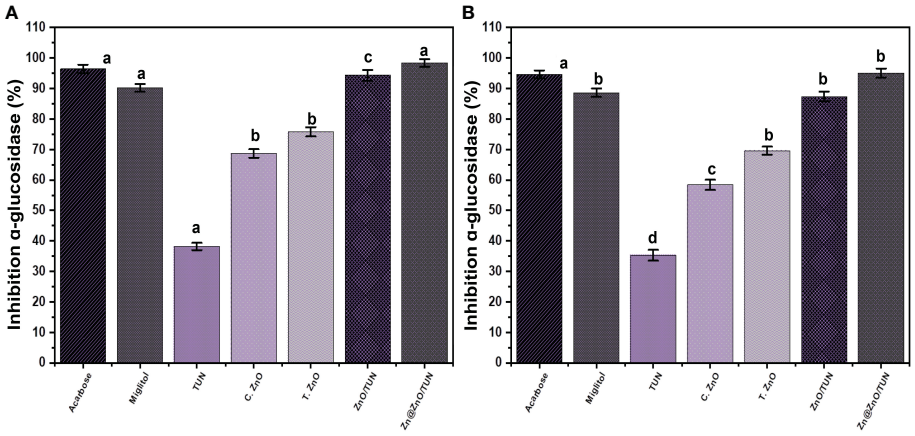

FIGURE 8
The inhibition properties of TUN, C.ZnO, T.ZnO, ZnO/TUN, and Zn@ZnO/TUN structures against pancreatic **(A)** and Murine intestinal **(B)** α-glucosidase enzyme. The values are the averages of 5 replicates, the error bars indicate the standard error of means, and different letters specify a statistical difference between the means (P<0.05).

3.3.4 Murine intestinal α-glucosidase inhibition

The inhibitory impacts of TUN, C.ZnO, T.ZnO, ZnO/TUN, and Zn@ZnO/TUN against the functional crude intestine α-glucosidase enzyme have been investigated along with the earlier investigated commercialized forms for a more feasible analysis. The findings demonstrate a significant inhibitory effect of Zn@ZnO/TUN (95.1 ± 1.5%) on the activity of the crude intestine α-glucosidase enzymes. The therapeutic value of Zn/CSR is much greater than the observed impacts of miglitol (88.6 ± 1.42%) and similar to the reported performance of acarbose (94.6 ± 1.34%) medications (Figure 8B). The synthesized T.ZnO (69.6 ± 1.3%) and ZnO/TUN (87.4 ± 1.6%) still have stronger inhibitory effects than

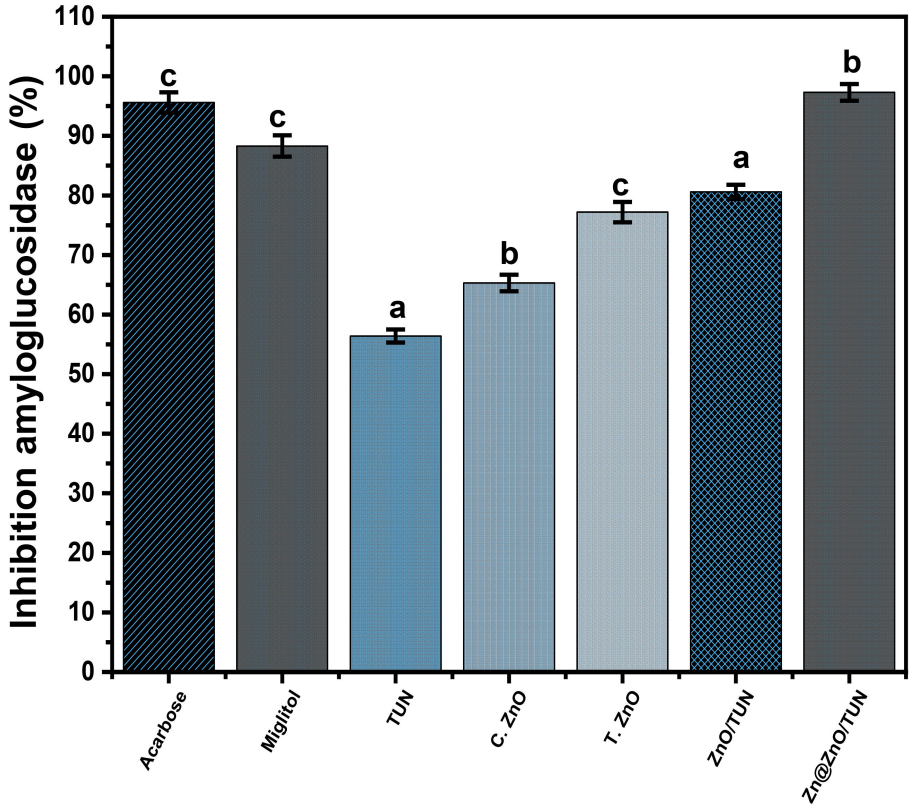

FIGURE 9
The amyloglucosidase inhibition activities of TUN, C.ZnO, T.ZnO, ZnO/TUN, and Zn@ZnO/TUN assessed materials. The values are the averages of 5 replicates, the error bars indicate the standard error of means, and different letters specify a statistical difference between the means (P<0.05).

both TUN (35.3 ± 1.8%) and C.ZnO (58.4 ± 1.7%) (Figure 8B). The properties of the synthesized Zn@ZnO/TUN hybrid, as established earlier, are sufficient considering the established health adverse effects of conventional medications and their high manufacturing cost. In general, green zinc metallic nanoparticles have significant potential as antidiabetic agents and have a substantial impact on reducing blood sugar concentrations. In addition, synthesized nanomaterials exhibit significant improvements in the function of insulin-related receptors, glucokinase genes, blood insulin levels, and glucokinase activity (Alkaladi et al., 2014).

3.3.5 Amyloglucosidase inhibition

The amyloglucosidase enzyme is highly efficient in facilitating the disintegration of complicated starch molecules and enhancing the digestion efficiencies of the resulting simple molecules. Consequently, the use of affordable, efficient, and secure synthesized materials that inhibit amyloglucosidase will greatly reduce the conversion of complicated sugar molecules into less complicated versions (Dhobale et al., 2008). The amyloglucosidase inhibitory % were determined by analyzing TUN, C.ZnO, T.ZnO, ZnO/TUN, and Zn@ZnO/TUN were found to be 56.4 ± 1.1%, 65.4 ± 1.27%, 77.2 ± 1.7%, 80.6 ± 1.2%, and 97.3 ± 1.4%, respectively (Figure 9). Nevertheless, all the examined nanostructures (TUN, C.ZnO, T.ZnO, ZnO/TUN, and Zn@ZnO/TUN) have significant inhibitory impacts on the amyloglucosidase enzyme; only the Zn/CSR hybrid material exhibits greater activity compared to either miglitol (88.3 ± 1.83%) or acarbose (95.6 ± 1.72%) medications (Figure 9). Hence, the Zn@ZnO/TUN hybrid, which consists of green-fabricated metallic zinc nanoparticles supported on a TUN substrate, can be suggested as a highly effective antidiabetic agent. This hybrid material is characterized by its inexpensive price of manufacturing, excellent biocompatibility, negligible adverse effects, and potent inhibition of frequently encountered oxidizing enzymes.

3.4 Cytotoxicity properties

The biologic compatibility, along with the safety of Zn@ZnO/TUN was evaluated by investigation for their cytotoxic impacts on conventional colorectal fibroblast cells (CCD-18Co). The toxicological properties of Zn@ZnO/TUN have been assessed in HCT-116 human colorectal tumor cells to identify their potential as a tumor suppressor. Concerning the harmful impact of Zn@ZnO/TUN against CCD-18Co normal cells, its structure possesses significant biological compatibility and bio-safety characteristics throughout the tested dose spectrum (20 to 100 µg/L). The tracked viability % when exposed to the greatest investigated dose of the Zn@ZnO/TUN particulates is 96.3%. With respect to the cytotoxic effects of liberated unloaded particulates upon HCT-116 cells, the synthesized hybrid material in the form of unbound particulates exhibits notable cytotoxicity towards the cancerous cells, particularly at administered doses exceeding 500 µg/mL. The results reveal that the administration of Zn@ZnO/TUN (500 µg/mL) caused considerable cytotoxicity effects with 47.3% cell viability, 52.7% inhibiting %, and 188 µg/mL IC-50.

4 Conclusion

Turbinaria ornata marine macro-algae (TUN) were successfully mediated with zinc/ZnO blended nanoparticles using the derived extract and its phytochemicals. The obtained green nano- and bio-composite (Zn@ZnO/TUN) was applied effectively as an affordable and biocompatible antioxidant and antidiabetic agent in comparison with the commercialized forms. The Zn@ZnO/TUN structure revealed enhanced scavenging efficiencies against the essential ROS ((DPPH (88.2 ± 1.44%), nitric oxide (92.7 ± 1.71%), ABTS (90.5 ± 1.8%), and $O_2^{\bullet-}$ (30.6 ± 1.32%) in comparison with either ascorbic acid or its individual components or ZnO. This was also reported during the inhibition reactions of the most effective oxidizing enzymes, considering the common medications (miglitol and acarbose), including commercial α-amylase (88.7 ± 1.3%), α-glucosidase (98.4 ± 1.3%), and amyloglucosidase (97.3 ± 1.4%)) and crude (α-amylase (66.2 ± 1.4%) and α-glucosidase (95.1 ± 1.5%)) forms. This demonstrates the significance of the green synthesis process of the metallic zinc in complex with algae-derived vial chemicals, in addition to the application of the algal structure as support. Also, induce the potential implementation of the composite in commercial and realistic studies, considering the biological factors across deep *in-vivo* studies.

Data availability statement

The raw data supporting the conclusions of this article will be made available by the authors, without undue reservation.

Ethics statement

Ethical approval was not required for the studies on animals in accordance with the local legislation and institutional requirements because only commercially available established cell lines were used.

Author contributions

AD: Formal analysis, Methodology, Resources, Software, Validation, Visualization, Writing – original draft, Writing – review & editing. KE: Conceptualization, Methodology, Resources, Writing – original draft, Writing – review & editing. AE-S: Funding acquisition, Investigation, Methodology, Project administration, Resources, Validation, Writing – original draft. WA: Investigation, Validation, Writing – original draft, Writing – review & editing. SB: Formal analysis, Methodology, Validation, Visualization, Writing – review & editing. MA: Conceptualization, Data curation, Formal analysis, Investigation, Methodology, Project administration, Resources, Software, Supervision, Validation, Visualization, Writing – original draft, Writing – review & editing.

Funding

The author(s) declare that financial support was received for the research, authorship, and/or publication of this article. The authors extend their appreciation to King Saud University for funding this work through Researchers Supporting Project number (RSP2024R133), King Saud University, Riyadh, Saudi Arabia.

Conflict of interest

The authors declare that the research was conducted in the absence of any commercial or financial relationships that could be construed as a potential conflict of interest.

Publisher's note

All claims expressed in this article are solely those of the authors and do not necessarily represent those of their affiliated organizations, or those of the publisher, the editors and the reviewers. Any product that may be evaluated in this article, or claim that may be made by its manufacturer, is not guaranteed or endorsed by the publisher.

Supplementary material

The Supplementary Material for this article can be found online at: https://www.frontiersin.org/articles/10.3389/fmars.2024.1444618/full#supplementary-material

References

Abdel Salam, M., Mokhtar, M., Albukhari, S. M., Baamer, D. F., Palmisano, L., Jaremko, M., et al. (2022). Synthesis and characterization of green znO@ polynaniline/bentonite tripartite structure (G. Zn@ PN/BE) as adsorbent for as (V) ions: integration, steric, and energetic properties. *Polym* 14, 2329. doi: 10.3390/polym14122329

Abukhadra, M. R., AlHammadi, A. A., Khim, J. S., Ajarem, J. S., and Allam, A. A. (2022). Enhanced decontamination of Levofloxacin residuals from water using recycled glass based a green zinc oxide/mesoporous silica nanocomposite; adsorption and advanced oxidation studies. *J. @ Cleaner. Product.* 356, 131836. doi: 10.1016/j.jclepro.2022.131836

Ahmed, Z. B., Hefied, F., Yousfi, M., Demeyer, K., and Vander Heyden, Y. (2022). Study of the antioxidant activity of *Pistacia atlantica Desf.* Gall extracts and evaluation of the responsible compounds. *Bio. Sys. Eco.* 100, 104358. doi: 10.1016/j.bse.2021.104358

Ali, A. A., Ahmed, F., Taher, H. S., Temraz, T. A., and Sami, M. (2024). Antimicrobial and antioxidant activities of some selected seaweeds species from the western coast of the northern Egyptian red sea. *Egyptian. J. Aquat. Biol. Fisheries.* 28, 609-630. doi: 10.21608/ejabf.2024.350010

Alkaladi, A., Abdelazim, A. M., and Afifi, M. (2014). Antidiabetic activity of zinc oxide and silver nanoparticles on streptozotocin-induced diabetic rats. *Inter. J. mole. Sci.* 15, 2015–2023. doi: 10.3390/ijms15022015

Alreshidi, M., Badraoui, R., Adnan, M., Patel, M., Alotaibi, A., Saeed, M., et al. (2023). Phytochemical profiling, antibacterial, and antibiofilm activities of *Sargassum* sp.(brown algae) from the Red Sea: ADMET prediction and molecular docking analysis. *Algal. Res.* 69, 102912. doi: 10.1016/j.algal.2022.102912

Ansari, A., Ali, A., Khan, N., Umar, M. S., and Owais, M. (2022). Synthesis of steroidal dihydropyrazole derivatives using green ZnO NPs and evaluation of their anticancer and antioxidant activity. *Steroids* 188, 109113. doi: 10.1016/j.steroids.2022.109113

Arvanag, M. F., Bayrami, A., Habibi-Yangjeh, A., and Pouran, S. R. (2019). A comprehensive study on antidiabetic and antibacterial activities of ZnO nanoparticles biosynthesized using *Silybum marianum L* seed extract. *Mater. Sci. Eng. C.* 97, 397–405. doi: 10.1016/j.msec.2018.12.058

Asmat, U., Abad, K., and Ismail, K. (2016). Diabetes mellitus and oxidative stress—A concise review. *Saudi. Pharm. J.* 24, 547–553. doi: 10.1016/j.jsps.2015.03.013

Atugoda, T., Gunawardane, C., Ahmad, M., and Vithanage, M. J. C. (2021). Mechanistic interaction of ciprofloxacin on zeolite modified seaweed (Sargassum crassifolium) derived biochar: Kinetics, isotherm and thermodynamics. *Chemosphere* 281, 130676. doi: 10.1016/j.chemosphere.2021.130676

Behl, T., Kaur, I., Sehgal, A., Sharma, E., Kumar, A., Grover, M., et al. (2021). Unfolding Nrf2 in diabetes mellitue. *Mol. Bio. Rep.* 48, 927–939. doi: 10.1007/s11033-020-06081-3

Bharath, B., Perinbam, K., Devanesan, S., AlSalhi, M. S., and Saravanan, M. (2021). Evaluation of the anticancer potential of Hexadecanoic acid from brown algae *Turbinaria ornata* on HT–29 colon cancer cells. *J. Mol. Structure.* 1235, 130229. doi: 10.1016/j.molstruc.2021.130229

Billacura, M. P., Cripps, M. J., Hanna, K., Sale, C., and Turner, M. D. (2022). β-alanine scavenging of free radicals protects mitochondrial function and enhances both insulin secretion and glucose uptake in cells under metabolic stress. *Adv. Redox Res.* 6, 100050. doi: 10.1016/j.arres.2022.100050

Botes, L. (2003). *Phytoplankton identification catalogue: Saldanha Bay, South Africa, April 2001* (London: IMO, Global Ballast Management Programme).

Dappula, S. S., Kandrakonda, Y. R., Shaik, B., Mothukuru, S. L., Lebaka, V. R., Mannarapu, M., et al. (1273). Biosynthesis of zinc oxide nanoparticles using aqueous extract of *Andrographis alata*: Characterization, optimization and assessment of their antibacterial, antioxidant, antidiabetic and anti-Alzheimer's properties. *J. @ Mole. Str.* 2023), 134264. doi: 10.1016/j.molstruc.2022.134264

da Silva-Neto, M. L., de Oliveira, M. C., Dominguez, C. T., Lins, R. E., Rakov, N., de Araújo, C. B., et al. (2019). UV random laser emission from flexible ZnO-Ag-enriched electrospun cellulose acetate fiber matrix. *Sci. Rep.* 9, 11765. doi: 10.1038/s41598-019-48056-w

Dedvisitsakul, P., and Watla-Iad, K. (2022). Antioxidant activity and antidiabetic activities of Northern Thai indigenous edible plant extracts and their phytochemical constituents. *Heliyon* 8, 10740. doi: 10.1016/j.heliyon.2022.e10740

De Morais, M. G., Da Silva Vaz, B., De Morais, E. G., and Costa, J. A. V. (2015). Biologically active metabolites synthesized by microalgae. *BioMed. Res. Int.* 2015, 1–15. doi: 10.1155/2015/835761

Deng, J., Wang, J., Hu, H., Hong, J., Yang, L., Zhou, H., et al. (2022). Application of mesoporous calcium silicate nanoparticles as a potential SD carrier to improve the solubility of curcumin. *J. @ Dispersion. Sci. Techno.* 44, 1–9. doi: 10.1080/01932691.2022.2068567

Dhall, A., and Self, W. (2018). Cerium oxide nanoparticles: a brief review of their synthesis methods and biomedical applications. *Antioxidants* 7, 97. doi: 10.3390/antiox7080097

Dhobale, S., Thite, T., Laware, S. L., Rode, C. V., Koppikar, S. J., Ghanekar, R. K., et al. (2008). Zinc oxide nanoparticles as novel alpha-amylase inhibitors. *J. @ Appl. Phys.* 104, 094907. doi: 10.1063/1.3009317

Dmytryk, A., Saeid, A., and Chojnacka, K. (2014). Biosorption of microelements by *Spirulina*: towards technology of mineral feed supplements. *Sci. World J.* 2014, 1-15. doi: 10.1155/2014/356328

Dulla, J. B., King, S. K. P., and Yekula, P. K. (2018). Investigation on biosorption of Cd(II) onto *Gelidiella acerosa* (brown algae): Optimization(using RSM & ANN) and mechanistic studies. *DESALINATION. AND. Water Treat* 107, 195–206. doi: 10.5004/dwt

El Shafay, S. M., Ali, S. S., and El-Sheekh, M. M. (2016). Antimicrobial activity of some seaweeds species from Red sea, against multidrug resistant bacteria. *Egyptian. J. Aquat. Res.* 42, 65–74. doi: 10.1016/j.ejar.2015.11.006

Elshikh, M. S., and Al Farraj, D. A. (2024). Postharvest disease control in banana using organic extract from the brown alga Turbinaria ornata. *Physiol. Mol. Plant Pathol.* 131, 102283. doi: 10.1016/j.pmpp.2024.102283

Fauziee, N. A. M., Chang, L. S., Mustapha, W. A. W., Nor, A. R. M., and Lim, S. J. (2021). Functional polysaccharides of fucoidan, laminaran and alginate from Malaysian brown seaweeds (*Sargassum polycystum, Turbinaria ornata* and *Padina boryana*). *Int. J. Biol. Macromol.* 167, 1135–1145. doi: 10.1016/j.ijbiomac.2020.11.067

Fawzy, M. A., Darwish, H., Alharthi, S., Al-Zaban, M. I., Noureldeen, A., and Hassan, S. H. A. (2022). Process optimization and modeling of Cd2+ biosorption onto the free and immobilized Turbinaria ornata using Box–Behnken experimental design. *Sci. Rep.* 12, 110380. doi: 10.1038/s41598-022-07288-z

Fawzy, M. A., and Gomaa, M. (2020). Use of algal biorefinery waste and waste office paper in the development of xerogels: A low cost and eco-friendly biosorbent for the effective removal of congo red and Fe (II) from aqueous solutions. *J. Environ. Manage.* 262, 110380. doi: 10.1016/j.jenvman.2020.110380

Feldman, E. L., Callaghan, B. C., Pop-Busui, R., Zochodne, D. W., Wright, D. E., Bennett, D. L., et al. (2019). Diabetic neuropathy. *Nat. Rev. Dis. Primer.* 5, 1–18. doi: 10.1038/s41572-019-0092-1

Guiry, M. D., and Guiry, G. M. (2015). Algae Base (Galway: World-wide electronic publication). Available at: http://www.algaebase.org/search/species/detail/?species_id=W2e71be855867c31e.

Hajra, D., and Paul, S. (2018). Study of glucose uptake enhancing potential of fenugreek (*Trigonella foenum graecum*) leaves extract on 3T3 L1 cells line and evaluation of its antioxidant potential. *Pharmacognosy. Res.* 10, 347-353. doi: 10.4103/pr.pr_50_18

Hakim, M. M., and Patel, I. C. (2020). A review on phytoconstituents of marine brown algae. *Future J. Pharm. Sci.* 6, 129. doi: 10.1186/s43094-020-00147-6

Hamasaki, T., Kashiwagi, T., Imada, T., Nakamichi, N., Aramaki, S., Toh, K., et al. (2008). Kinetic analysis of superoxide anion radical-scavenging and hydroxyl radical-scavenging activities of platinum nanoparticles. *Langmuir* 24, 7354–7364. doi: 10.1021/la704046f

Harborne, J. B. (1973). *Phytochemical methods* (London: Chapman and Hall Ltd), 49–188.

Hasan, E. A., El-Hashash, M. A., Zahran, M. K., and El-Rafie, H. M. (2022). Comparative study of chemical composition, antioxidant and anticancer activities of both *Turbinaria* decurrens Bory methanol extract and its biosynthesized gold nanoparticles. *J. Drug Deliv. Sci. Technol.* 67, 103005. doi: 10.1016/j.jddst.2021.103005

Hsu, W. H., Chang, H. M., Lee, Y. L., Prasannan, A., Hu, C. C., Wang, J. S., et al. (2020). Biodegradable polymer-nanoclay composites as intestinal sleeve implants installed in digestive tract for obesity and type 2 diabetes treatment. *Mater. Sci. Eng.: C.* 110, 110676. doi: 10.1016/j.msec.2020.110676

Itroutwar, P. D., Govindaraju, K., Tamilselvan, S., Kannan, M., Raja, K., and Subramanian, K. S. (2019). Seaweed-based biogenic znO nanoparticles for improving agro-morphological characteristics of rice (Oryza sativa L.). *J. Plant Growth Regul.* 39, 717–728. doi: 10.1007/s00344-019-10012-3

Khairy, H. M., and El-Sheikh, M. A. (2015). Antioxidant activity and mineral composition of three Mediterranean common seaweeds from Abu-Qir Bay, Egypt. *Saudi. J. Biol. Sci.* 22, 623–630. doi: 10.1016/j.sjbs.2015.01.010

Kim, M. S., Jung, Y. S., Jang, D., Cho, C. H., Lee, S. H., Han, N. S., et al. (2022). Antioxidant capacity of 12 major soybean isoflavones and their bioavailability under simulated digestion and in human intestinal Caco-2 cells. *Food Chem.* 374, 131493. doi: 10.1016/j.foodchem.2021.131493

Kitture, R., Ghosh, S., More, P. A., Gaware, S., Datar, S., Chopade, B. A., et al. (2015). Curcumin-loaded, self-assembled aloevera template for superior antioxidant activity and trans-membrane drug release. *J. @ Nanosci. Nanotech.* 15, 4039–4045. doi: 10.1166/jnn.2015.10322

Lauritano, C., Andersen, J. H., Hansen, E., Albrigtsen, M., Escalera, L., Esposito, F., et al. (2016). Bioactivity screening of microalgae for antioxidant, anti-inflammatory, anticancer, anti-diabetes, and antibacterial activities. *Front. Mar. Sci.* 3. doi: 10.3389/fmars.2016.00068

Lawande, P. P., Sontakke, V. A., Kumbhar, N. M., Bhagwat, T. R., Ghosh, S., and Shinde, V. S. (2017). Polyhydroxylated azetidine iminosugars: Synthesis, glycosidase inhibitory activity and molecular docking studies. *Bioorganic. Med. Chem. Lett.* 27, 5291–5295. doi: 10.1016/j.bmcl.2017.10.025

Liu, Y., Ying, D., Cai, Y., and Le, X. (2017). Improved antioxidant activity and physicochemical properties of curcumin by adding ovalbumin and its structural characterization. *Food Hydrocolloids.* 72, 304–311. doi: 10.1016/j.foodhyd.2017.06.007

Maggio, A., Alduina, R., Oddo, E., Piccionello, A. P., and Mannino, A. M. (2022). Antibacterial activity and HPLC analysis of extracts from Mediterranean brown algae. *Plant Biosystems-An. Int. J. Dealing. all Aspects. Plant Biol.* 156, 43–50. doi: 10.1080/11263504.2020.1829737

Malik, A. R., Sharif, S., Shaheen, F., Khalid, M., Iqbal, Y., Faisal, A., et al. (2022). Green synthesis of RGO-ZnO mediated *Ocimum basilicum* leaves extract nanocomposite for antioxidant, antibacterial, antidiabetic and photocatalytic activity. *J. @ Saudi. Chem. Soc.* 26, 101438. doi: 10.1016/j.jscs.2022.101438

Meer, B., Andleeb, A., Iqbal, J., Ashraf, H., Meer, K., Ali, J. S., et al. (2022). Bio-assisted synthesis and characterization of zinc oxide nanoparticles from *lepidium sativum* and their potent antioxidant, antibacterial and anticancer activities. *Biomolecules* 12, 855. doi: 10.3390/biom12060855

Mellouk, Z., Benammar, I., Krouf, D., Goudjil, M., Okbi, M., and Malaisse, W. (2017). Antioxidant properties of the red alga *Asparagopsis taxiformis* collected on the North West Algerian coast. *Exp. Ther. Med.* 13, 3281–3290. doi: 10.3892/etm.2017.4413

Naureen, B., Miana, G. A., Shahid, K., Asghar, M., Tanveer, S., Faheem, M., et al. (2021). Iron (III) and zinc (II) metal alkaloid complexes: synthesis, characterization and biological activities. *Malaysian. J. @ Chem.* 23, 55–73.

Nguyen, A. N., Van Ngo, Q., Quach, T. T. M., Ueda, S., Yuguchi, Y., Matsumoto, Y., et al. (2024). Fucoidan from brown seaweed Tubinaria decurrens: Structure and structure-anticancer activity relationship. *Int. J. Biol. Macromol.* 259, 129326. doi: 10.1016/j.ijbiomac.2024.129326

Noohpisheh, Z., Amiri, H., Farhadi, S., and Mohammadi-Gholami, A. (2020). Green synthesis of Ag-ZnO nanocomposites using *Trigonella foenum-graecum* leaf extract and their antibacterial, antifungal, antioxidant and photocatalytic properties. *Spectrochimica. Acta Part A. Mol. Biomol. Spec.* 240, 118595. doi: 10.1016/j.saa.2020.118595

Palanisamy, S., Vinosha, M., Marudhupandi, T., Rajasekar, P., and Prabhu, N. M. (2017). Isolation of fucoidan from *Sargassum polycystum* brown algae: Structural characterization, *in vitro* antioxidant and anticancer activity. *Int. J. Biol. Macromol.* 102, 405–412. doi: 10.1016/j.ijbiomac.2017.03.182

Pamungkas, D. B. P., Setyati, W. A., and Ryandini, D. (2024). Antibacterial Ability of Seaweed Endophytic Bacteria (*Turbinaria ornata, Sargassum crassifolium, and Sargassum polycystum*) Against Skin Disease Agents. *Trends Sci.* 21, 7282–7282. doi: 10.48048/tis.2024.7282

Parul, R., Kundu, S. K., and Saha, P. (2013). *In vitro* nitric oxide scavenging activity of methanol extracts of three Bangladeshi medicinal plants. *pharma. Innovation* 1, 83.

Prasad, S., and Lall, R. (2022). Zinc-curcumin based complexes in health and diseases: an approach in chemopreventive and therapeutic improvement. *J. @ Trace Elem. Med. Bio* 73, 127023. doi: 10.1016/j.jtemb.2022.127023

Rabie, A. M., Abukhadra, M. R., Rady, A. M., Ahmed, S. A., Labena, A., Mohamed, H. S., et al. (2020). Instantaneous photocatalytic degradation of malachite green dye under visible light using novel green Co–ZnO/algae composites. *Res. Chem. Intermediates.* 46, 1955–1973. doi: 10.1007/s11164-019-04074-x

Raj, C. T. D., Muthukumar, K., Dahms, H. U., James, R. A., and Kandaswamy, S. (2023). Structural characterization, antioxidant and anti-uropathogenic potential of biogenic silver nanoparticles using brown seaweed Turbinaria ornata. *Front. Microbiol.* 14. doi: 10.3389/fmicb.2023.1072043

Rehana, D., Mahendiran, D., Kumar, R. S., and Rahiman, A. K. (2017). *In vitro* antioxidant and antidiabetic activities of zinc oxide nanoparticles synthesized using different plant extracts. *Bioprocess. Biosyst. Engineer.* 40, 943–957. doi: 10.1007/s00449-017-1758-2

Robkhob, P., Ghosh, S., Bellare, J., Jamdade, D., Tang, I. M., and Thongmee, S. (2020). Effect of silver doping on antidiabetic and antioxidant potential of ZnO nanorods. *J. @ Trace Elements. Med. Bio* 58, 126448. doi: 10.1016/j.jtemb.2019.126448

Rosa, G. P., do Carmo, M., Barreto, M., Seca, A. M., and Pinto, D. (2022). *Pharmaceutical and H. Applications, Chemical Composition and Phytopharmaceuticals: An Overview of the Caulerpa and Cystoseira Genera. ustainable Global Resources of Seaweeds Volume 2: Food, Pharmaceutical and Health Applications*. Springer. 473–493.

Rudayni, H. A., Alenazi, N. A., Rabie, A. M., Aladwani, M., Alneghery, L. M., Abu-Taweel, G. M., et al. (2023). Biological characterization of microwave based synthesized ZnO and Ce doped ZnO nanoflowers impeded chitosan matrix with enhanced antioxidant and anti-diabetic properties. 2023. *Int. J. Biol. Macromol.* 242, 124713. doi: 10.1016/j.ijbiomac.2023.124713

Saad, A. M., Abukhadra, M. R., Ahmed, S. A. K., Elzanaty, A. M., Mady, A. H., Betiha, M. A., et al. (2020). Photocatalytic degradation of malachite green dye using chitosan supported ZnO and Ce–ZnO nano-flowers under visible light. *J. @ Enviro. Mana.* 258, 110043. doi: 10.1016/j.jenvman.2019.110043

Sagandira, C. R., Khasipo, A. Z., Sagandira, M. B., and Watts, P. (2021). An overview of the synthetic routes to essential oral anti-diabetes drugs. *Tetrahedron* 96, 132378. doi: 10.1016/j.tet.2021.132378

Sanap, S. P., Ghosh, S., Jabgunde, A. M., Pinjari, R. V., Gejji, S. P., Singh, S., et al. (2010). Synthesis, computational study and glycosidase inhibitory activity of polyhydroxylated conidine alkaloids—a bicyclic iminosugar. *Organic. Biomole. Chem.* 8, 3307–3315. doi: 10.1039/c004690f

Shaaban, S., Adam, M. S. S., and El-Metwaly, N. M. (2022). Novel organoselenium-based N-mealanilic acid and its zinc (II) chelate: Catalytic, anticancer, antimicrobial, antioxidant, and computational assessments. *J. @ Mole. Liquid.* 363, 119907. doi: 10.1016/j.molliq.2022.119907

Sharma, A., Nagraik, R., Sharma, S., Sharma, G., Pandey, S., Azizov, S., et al. (2022). Green synthesis of ZnO nanoparticles using *Ficus palmata*: Antioxidant, antibacterial and antidiabetic studies. *Results. Chem.* 4, 100509. doi: 10.1016/j.rechem.2022.100509

Sharpe, E., Andreescu, D., and Andreescu, S. (2011). "Artificial nanoparticle antioxidants," in *Oxidative stress: diagnostics, prevention, and therapy*. ACS Publication, 235–253.

Shu, G., Xu, D., Xie, S., Chang, L. J., Liu, X., Yang, J., et al. (2023). The antioxidant, antibacterial, and infected wound healing effects of ZnO quantum dots-chitosan biocomposite. *App. Sur. Sci.* 611, 155727. doi: 10.1016/j.apsusc.2022.155727

Singh, T. A., Sharma, A., Tejwan, N., Ghosh, N., Das, J., and Sil, P. C. (2021). A state of the art review on the synthesis, antibacterial, antioxidant, antidiabetic and tissue regeneration activities of zinc oxide nanoparticles. *Adv. Coll. Inter. Sci.* 295, 102495. doi: 10.1016/j.cis.2021.102495

Song, Y., Yang, F., Ma, M., Kang, Y., Hui, A., Quan, Z., et al. (2022). Green synthesized Se–ZnO/attapulgite nanocomposites using Aloe vera leaf extract: Characterization, antibacterial and antioxidant activities. *LWT* 165, 113762. doi: 10.1016/j.lwt.2022.113762

Trease, G. E., and Evans, W. C. (1989). *Pharmacognosy. 13th edn* (London: Balliere Tindall), pp176–pp180.

Velsankar, K., Venkatesan, A., Muthumari, P., Suganya, S., Mohandoss, S., and Sudhahar, S. (2022). Green inspired synthesis of ZnO nanoparticles and its characterizations with biofilm, antioxidant, anti-inflammatory, and anti-diabetic activities. *J. @ Mole. Str.* 1255, 132420. doi: 10.1016/j.molstruc.2022.132420

Vinotha, V., Iswarya, A., Thaya, R., Govindarajan, M., Alharbi, N. S., Kadaikunnan, S., et al. (2019). Synthesis of ZnO nanoparticles using insulin-rich leaf extract: Anti-diabetic, antibiofilm and anti-oxidant properties. *J. @ Photochem. Photobio. B: Biol.* 197, 111541.

Xie, J., Wang, N., Dong, X., Wang, C., Du, Z., Mei, L., et al. (2018). Graphdiyne nanoparticles with high free radical scavenging activity for radiation protection. *ACS Appl. Mater. Interfaces.* 11, 2579–2590. doi: 10.1021/acsami.8b00949

Yang, X., Wang, J., El-Sherbeeny, A. M., AlHammadi, A. A., Park, W.-H., and Abukhadra, M. R. (2022). Insight into the adsorption and oxidation activity of a ZnO/piezoelectric quartz core-shell for enhanced decontamination of ibuprofen: Steric, energetic, and oxidation studies. *Chem. Eng. J.* 431, 134312. doi: 10.1016/j.cej.2021.134312

Yilmazer-Musa, M., Griffith, A. M., Michels, A. J., Schneider, E., and Frei, B. (2012). Grape seed and tea extracts and catechin 3-gallates are potent inhibitors of α-amylase and α-glucosidase activity. *J. @ Agric. Food Chem.* 60, 8924–8929. doi: 10.1021/jf301147n

Yusof, N. A. A., Zain, N. M., and Pauzi, N. (2019). Synthesis of ZnO nanoparticles with chitosan as stabilizing agent and their antibacterial properties against Gram-positive and Gram-negative bacteria. *Inter. J. @ bio. Macromol.* 124, 1132–1136. doi: 10.1016/j.ijbiomac.2018.11.228